IntraVital 3, e27935; February; © 2014 Landes Bioscience

Optimization of the dorsal skinfold window chamber model and multi-parametric characterization of tumor-associated vasculature

Azusa Maeda and Ralph S DaCosta*

Ontario Cancer Institute; University Health Network; Toronto, ON Canada; Department of Medical Biophysics; University of Toronto; Toronto, ON Canada

Keywords: dorsal skinfold window chamber model, vascular imaging, fluorescence, perfusion, vascularity, tortuosity

The dorsal skinfold window chamber (DSWC) model is a unique tool that enables analysis of various aspects of tumor biology and therapeutic response. Although the protocol for the murine DSWC model is standardized, certain tumors fail to grow or require a particular environment to promote growth. Given such limitations, we optimized the DSWC model for a slow-growing tumor that regresses spontaneously in the standard protocol. We further characterized the vascular network in the tumor model compared with that of non-tumor-bearing mice and observed significant differences in multiple parameters related to vascular structure and function.

Implantation of a dorsal skinfold window chamber (DSWC) in rodents enables microscopic observation of living tissue, such as that of a tumor model. A major advantage of the technique is the ability to track dynamic changes of the tumor and its microenvironment over a period of 2–3 wk.[1] Given the ability to track changes over time, the DSWC model has been used to monitor stages of tumor-stromal interaction,[2,3] tumor-induced angiogenesis[4,5] and tumor response to treatments such as vascular-targeting agents,[6-8] nanoparticles,[9,10] and radiation therapy.[11,12] The DSWC model is particularly well suited for studies of vascular network, since it enables examination of vascular function and structure with sufficient resolution when combined with fluorescence microscopy.[13]

To prepare the DSWC mouse model for studying tumors and their vasculature, fluorescent tumor cells are typically implanted under the glass of the chambers at the time of the window installation[14] or after a recovery period of 48 h.[4] However, a large number of tumor cells (10^6 to 10^7) must be injected to ensure tumor growth; moreover, the tumor cells may fail to grow and undergo apoptosis in some cases.[15] To avoid tumor regression, it is recommended to house the mice in an environmental chamber with elevated temperature and humidity (34 °C, 50% humidity) to ensure tumor growth.[14] However, 34 °C is beyond the optimal temperature of 20–22 °C for group-housed mice and may negatively impact homeostasis.[16]

Here, we investigated an alternative approach to promote the growth of tumor cells that may otherwise undergo spontaneous regression when implanted directly into the DSWC model. A human pancreatic cancer cell line, BxPC-3, was chosen for this study because it has a long tumor growth latency period after subcutaneous injection.[17] Furthermore, using the optimized method of tumor inoculation in the DSWC model, we characterized the structure and function of tumor-associated vasculature and normal vasculature, as a demonstration of a reproducible and quantitative method for vasculature analysis.

DsRed fluorescent BxPC-3 human pancreatic cancer cells (Anticancer Inc.) were grown at 37 °C and 5% CO_2 in RPMI 1640 medium supplemented with 2 mM L-glutamine, 10% fetal bovine serum and 1% Penicillin Streptomycin (GIBCO BRL). DsRed-BxPC-3 cells, prepared in 1:1 PBS:Matrigel (BD Biosciences) solution, were injected into eight-week old NOD-Rag1 IL2rg mice (kindly provided by Dr. Richard Hill, Ontario Cancer Institute) as follows: 500 000 cells at the time of DSWC installation, or 100 000 cells subcutaneously into the dorsal skin. In the latter method, the DSWC surgery was performed 10 d after the tumor injection when the tumors became palpable. Non-tumor-bearing mice were also prepared as a normal control group. Window chambers were surgically implanted into the dorsal skinfold of anesthetized mice using established methods.[14] All animal procedures were conducted in accordance with appropriate regulatory standards under protocol #2407 approved by the University Health Network Institutional Animal Care and Use Committee.

Following a recovery period of 3–5 d post-DSWC installation, mice were imaged using a stereomicroscope (MZ FLIII, Leica Microsystems) and confocal fluorescence microscope (LS510 Meta, Carl Zeiss). A 4× objective lens was used for the confocal imaging, which resulted in an optical thickness of 520 µm for each image. 2MDa FITC-Dextran (FD2000S, Sigma-Aldrich) was injected into the tail vein prior to each imaging session to

*Correspondence to: Ralph S DaCosta; Email: rdacosta@uhnres.utoronto.ca
Submitted: 11/25/2013; Revised: 01/20/2014; Accepted: 01/21/2014; Published Online: 02/04/2014
Citation: Maeda A, DaCosta RS. Optimization of the dorsal skinfold window chamber model and multi-parametric characterization of tumor-associated vasculature. IntraVital 2014; 3:e27935; http://dx.doi.org/10.4161/intv.27935

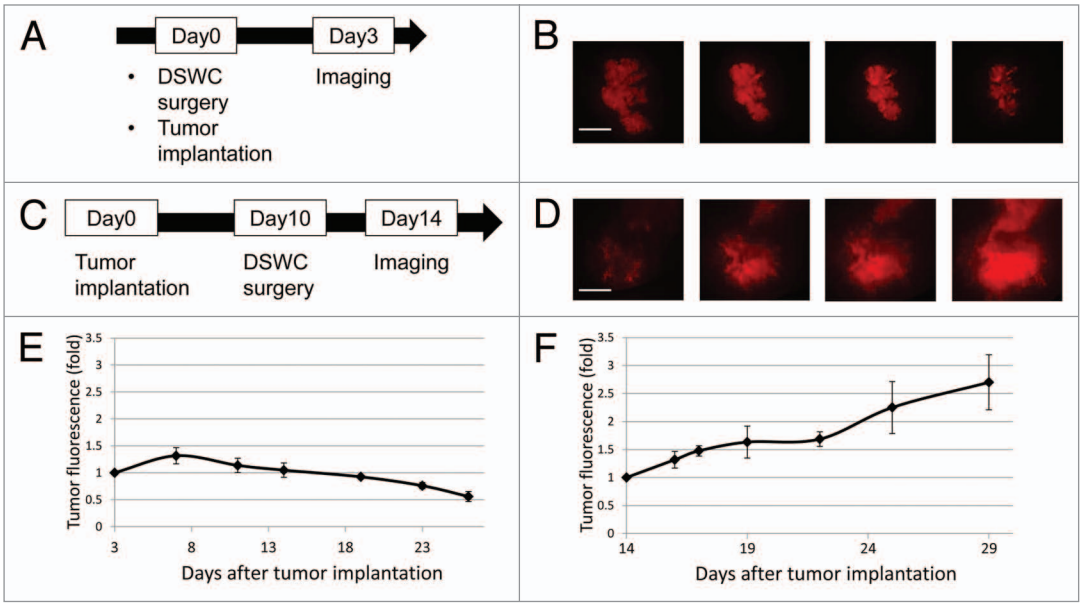

Figure 1. (**A**) Tumor implantation protocol, in which DsRed fluorescent BxPC-3 cells were injected at the time of the DSWC surgery, and (**B**) corresponding change in tumor fluorescence over time, at 7, 14, 19, and 26 d after tumor implantation. Scale bar = 2 mm. (**C**) Optimized tumor implantation protocol, in which tumor cells were implanted subcutaneously prior to the DSWC surgery, and (**D**) corresponding change in tumor fluorescence over time, at 16, 22, 25, and 29 d after tumor implantation. Scale bar = 2 mm. (**E**) Quantified tumor fluorescence intensity for tumors that were implanted at the time of DSWC surgery (n = 3). (**F**) Quantified fluorescence intensity for tumors that were implanted 10 d prior to the DSWC surgery (n = 5). The values in (**E**) and (**F**) were normalized to the first day of imaging and expressed as fold changes. Error bars = SEM.

identify functional vasculature using the confocal fluorescence microscope. Each mouse was imaged serially for up to 26 d following the DSWC surgery. A custom mouse restrainer with heating element was used during imaging to prevent motion artifacts and maintain physiological temperature of the mice.[12]

Fluorescence images were processed and analyzed using ImageJ and MATLAB. Tumor fluorescence intensity was measured based on the images acquired using the stereomicroscope. Specifically, the images were processed in MATLAB, displayed in an alternative color-map, and the sum of all pixel intensities was calculated. To obtain measurements of functional vessel density from the confocal fluorescence images of the vascular network, the raw fluorescence images were binarized using a MATLAB implementation of Otsu's method[18]. The binarized images were then analyzed to calculate % pixel count within a defined region of interest (ROI), as a measure of functional vessel density. The confocal fluorescence images were processed separately for skeletonization using a smoothing algorithm in ImageJ, followed by a skeletonization algorithm (AnalyzeSkeleton plugin for ImageJ[19]), which calculates the number of branches, number of junctions, length of each branch and the straight-line distance between the end points of each branch (Euclidian distance). Based on these measurements, total branch length and tortuosity (calculated as branch length/Euclidean distance) were measured for all the branches within the ROI. The size of the ROI was kept consistent for all images (1.5 mm ´ 1.5 mm). Data are represented as mean ± SEM and Student's two- sample *t* test was used to determine significance.

To examine the kinetics of tumor growth in the DSWC, tumor fluorescence was measured over the course of 2–3 wk following the DSWC surgery. DsRed fluorescent BxPC-3 tumors were approximately 3 mm in diameter at the time of imaging for both injection methods (**Fig. 1A–D**). As seen in **Figure 1E**, the BxPC-3 cells that were injected at the time of window chamber surgery regressed spontaneously over the course of 26 d, reaching approximately half of the fluorescence intensity at the endpoint. In comparison, tumors that were grown subcutaneously prior to the window chamber surgery grew steadily (**Fig. 1F**), reaching almost three times the original tumor fluorescence intensity. The latter method was determined to be optimal based on the growth curve, and was used for the following studies.

Confocal fluorescence microscopy was used to image perfused vasculature in non-tumor-bearing (normal) and tumor-bearing mice, using FITC-Dextran as a contrast agent (**Fig. 2A and B**). The raw fluorescence images were segmented into binary images for quantification of functional vessel area, and skeletonized for quantification of branch length and tortuosity (**Fig. 2C and D**). The ROI in the tumor-bearing mice was chosen within the DsRed fluorescent BxPC-3 tumor to characterize tumor-associated vasculature, and the ROI of the same size was used for quantification of the normal vasculature.

Within the ROI of the same size, functional vessel area was significantly higher in the normal mice compared with tumor-bearing mice at each time point, reflecting the extent of perfusion in the ROI (**Fig. 3A**). The difference was most significant at 21 d following the window chamber installation, with more than an 8-fold difference between normal and tumor-associated vasculature. Of note, the functional vessel area takes into consideration the diameter of each vessel; thus, any changes in the functional vessel area can be due to the differences in the

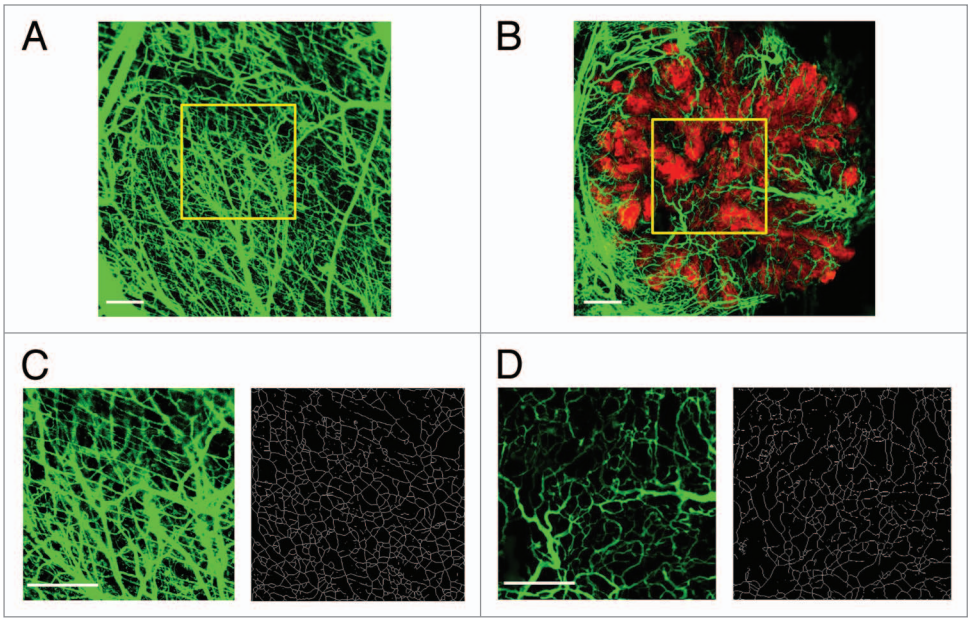

Figure 2. (**A**) Representative fluorescence image of the normal vasculature 21 d after the DSWC surgery. (**B**) Representative fluorescence image of the tumor-associated vasculature 21 d after the DSWC surgery. The vasculature was visualized by FITC-Dextran (green), and the DsRed-BxPC-3 tumor is shown in red. Scale bar = 500 μm. (**C**) Magnified images of the area highlighted in yellow for the normal vasculature. The raw fluorescence image (right) was used to quantify functional vessel area, and the skeletonized image (left) was used to quantify branch length and tortuosity. Scale bar = 500 μm. (**D**) Magnified images of the area highlighted in yellow for the tumor vasculature. The raw fluorescence image (right) was used to quantify functional vessel area, and the skeletonized image (left) was used to quantify branch length and tortuosity. Scale bar = 500 μm.

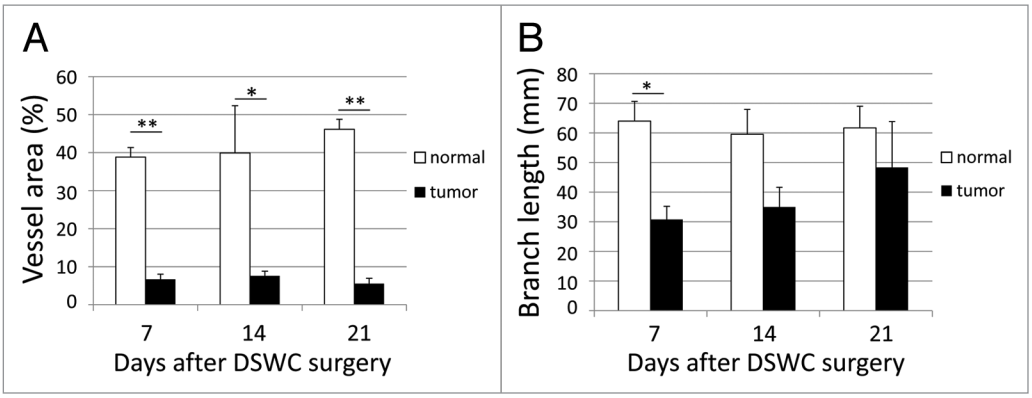

Figure 3. (**A**) Functional vessel area calculated based on binarized fluorescence images for normal (n = 5) and tumor (n = 4) vasculature. The values were calculated as % area within the ROI that is filled with the fluorescence signal. *: $P < 0.05$, **: $P < 0.01$. Error bars = SEM (**B**) Total branch length calculated based on the skeletonized images of the vasculature for normal (n = 5) and tumor (n = 4) vasculature. *$P < 0.05$. Error bars = SEM.

number of vessels as well as in the thickness of each vessel within the ROI.

In order to further analyze vasculature, the raw data was processed using a smoothing algorithm to remove noise, and further skeletonized. The skeletonization algorithm enabled analysis of branch length, which is a measure of vascularity, independent of the diameter of each vessel. The calculated total branch length of the normal vasculature was significantly higher than that of the tumor at 7 d following the window chamber installation, with an over 2-fold difference (**Fig. 3B**). Moreover, there was a trend of increasing branch length in the tumor over the course of two weeks, which may indicate tumor-induced angiogenesis.

The skeletonized images described above were also used to calculate vascular tortuosity. Vascular tortuosity of the tumors is expected to be higher than that of the control,[20] and is of particular importance because it may indicate malignant disease[21,22] and treatment response.[23] The minimum value of tortuosity is 1, which represents a straight line. As seen in **Figure 4A**, the average tortuosity of the tumor-associated vasculature was higher than that of the normal, with the most significant difference seen at 21 d following the DSWC surgery. Over 75% of

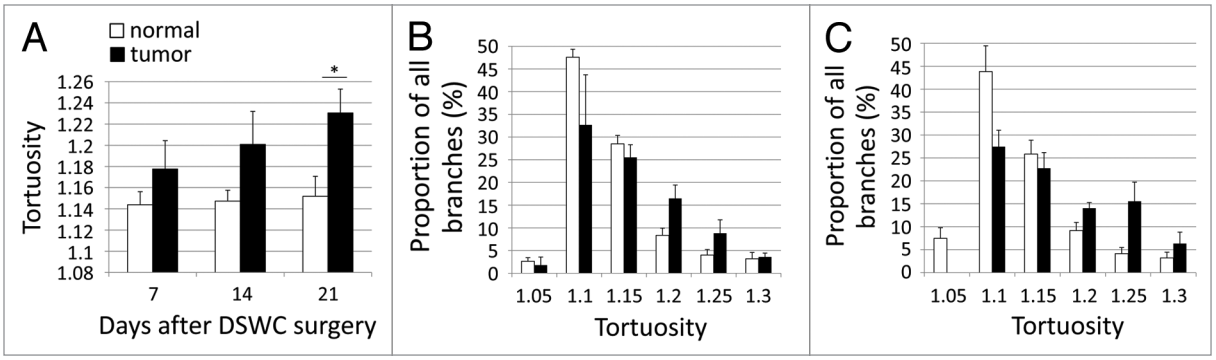

Figure 4. (**A**) Average tortuosity of normal (n = 5) and tumor (n = 4) vasculature. Frequency histogram between tortuosity value of 1.05 and 1.3 measured at (**B**) day 7 and (**C**) day 21 following the DSWC surgery for normal (white bars) and tumor (black bars) vasculature. The number of branches that fall within a particular bin for tortuosity value is expressed as a % of the total number of branches. *$P < 0.05$. Error bars = SEM.

the normal vasculature fell within the tortuosity range of 1.05–1.15 with an average of 1.14–1.15, while the tortuosity of tumor-associated vasculature ranged widely between 1.1–1.25 (**Fig. 4B and C**). Furthermore, there was a steady increase in the average tortuosity of the tumor-associated vasculature from 1.18 to 1.23 at days 7 and 21, respectively, but not of the normal vasculature. This trend can also be seen by the frequency histogram, which shows a general shift toward higher tortuosity in the tumor-associated vasculature between days 7 and 21, while that of the normal vasculature remains similar.

As multiple applications of the DSWC tumor model emerge, there is a need to optimize the technique to recapitulate the tumor biology of a traditional xenograft model. This is particularly important for tumors, such as those derived from the human pancreatic BxPC-3 cell line, which do not grow in the DSWC as they would in the subcutaneous xenograft model. This could be due to reduced temperature within the DSWC as it suspends the skin away from the body such that the skin is not maintained at normal body temperature.[24] Given such limitations, it is common to house the animals in warm conditions, or implant tumor fragments to achieve better tumor growth.[25] However, the latter technique, which is commonly used in rats, may be technically challenging in mice due to the small DSWC size. We investigated an alternative approach to promote tumor growth in the DSWC model and demonstrated that injecting the tumor cells subcutaneously prior to the window chamber surgery enabled BxPC-3 tumor growth over the course of three weeks. This modified technique is technically less complex than implanting tumor fragments into a small field of the DSWC, and thus recommended as an optimal approach for slow-growing tumors that may be of interest for studying particular therapies or tumors and/or their microenvironment.

Moreover, we demonstrated that simple algorithms can be applied to measure multiple parameters that are relevant to the structure and function of the vascular network. Although a similar quantification method has been previously described,[26] we utilized a skeletonization method to facilitate analysis of the vascular networks. The vascular features described here, which are measures of perfusion, vascularity and tortuosity, have implications for tumor biology and treatment response. For example, treatment of tumors with vascular targeting drugs such as anti-VEGF agent results in decreased tortuosity, vessel length and density, leading to "vascular normalization," an indication of improved tumor metabolism and drug delivery.[23] Our data showed that the vascular network in the optimized tumor model was significantly different than that of the control. Specifically, the tumor area was not as well-perfused or vascularized compared with a normal area of the same size, and the tumor-associated vasculature was more tortuous than the normal vasculature. Interestingly, our data also demonstrated that vessel length and tortuosity increased as tumors grew, which may be an indication of tumor-induced angiogenesis. In fact, this observation is in agreement with a review of commonly used pancreatic cancer cell lines, in which BxPC-3 cells were shown to have high angiogenic potential compared with other pancreatic cancer cell lines.[17] To better distinguish true branching from overlapping vessels in a two-dimensional image, 3D imaging and image reconstruction methods may be used in the future.[27] The image quantification method can also be applied in various orthotopic intravital models, such as an orthotopic pancreatic or abdominal window chamber models.[28]

A growing number of laboratories utilize the DSWC model for studies of tumor and vascular biology. The methods described here address an issue associated with the standard protocol for intravital imaging, provides an alternative approach to optimize the model, and provides a method to quantitatively analyze tumors and their vascular network, all aimed to help address therapeutically relevant questions.

Disclosure of Potential Conflicts of Interest

No potential conflicts of interest were disclosed.

Acknowledgments

We thank Leigh Conroy for her help with the MATLAB algorithms and Dr Iris Kulbatski for her help with editing the manuscript. This work was supported by funding provided to R. DaCosta by the Canadian Institutes for Health Research.

References

1. Koehl GE, Gaumann A, Geissler EK. Intravital microscopy of tumor angiogenesis and regression in the dorsal skin fold chamber: mechanistic insights and preclinical testing of therapeutic strategies. Clin Exp Metastasis 2009; 26:329-44; PMID:19190882; http://dx.doi.org/10.1007/s10585-008-9234-7
2. Alexander S, Koehl GE, Hirschberg M, Geissler EK, Friedl P. Dynamic imaging of cancer growth and invasion: a modified skin-fold chamber model. Histochem Cell Biol 2008; 130:1147-54; PMID:18987875; http://dx.doi.org/10.1007/s00418-008-0529-1
3. Alexander S, Weigelin B, Winkler F, Friedl P. Preclinical intravital microscopy of the tumour-stroma interface: invasion, metastasis, and therapy response. Curr Opin Cell Biol 2013; 25:659-71; PMID:23896198; http://dx.doi.org/10.1016/j.ceb.2013.07.001
4. Vajkoczy P, Ullrich A, Menger MD. Intravital fluorescence videomicroscopy to study tumor angiogenesis and microcirculation. Neoplasia 2000; 2:53-61; PMID:10933068; http://dx.doi.org/10.1038/sj.neo.7900062
5. Li CY, Shan S, Huang Q, Braun RD, Lanzen J, Hu K, Lin P, Dewhirst MW. Initial stages of tumor cell-induced angiogenesis: evaluation via skin window chambers in rodent models. J Natl Cancer Inst 2000; 92:143-7; PMID:10639516; http://dx.doi.org/10.1093/jnci/92.2.143
6. Tozer GM, Kanthou C, Parkins CS, Hill SA. The biology of the combretastatins as tumour vascular targeting agents. Int J Exp Pathol 2002; 83:21-38; PMID:12059907; http://dx.doi.org/10.1046/j.1365-2613.2002.00211.x
7. Seshadri M, Spernyak JA, Maiery PG, Cheney RT, Mazurchuk R, Bellnier DA. Visualizing the acute effects of vascular-targeted therapy in vivo using intravital microscopy and magnetic resonance imaging: correlation with endothelial apoptosis, cytokine induction, and treatment outcome. Neoplasia 2007; 9:128-35; PMID:17356709; http://dx.doi.org/10.1593/neo.06748
8. Winkler F, Kozin SV, Tong RT, Chae SS, Booth MF, Garkavtsev I, Xu L, Hicklin DJ, Fukumura D, di Tomaso E, et al. Kinetics of vascular normalization by VEGFR2 blockade governs brain tumor response to radiation: role of oxygenation, angiopoietin-1, and matrix metalloproteinases. Cancer Cell 2004; 6:553-63; PMID:15607960
9. Murphy EA, Majeti BK, Barnes LA, Makale M, Weis SM, Lutu-Fuga K, Wrasidlo W, Cheresh DA. Nanoparticle-mediated drug delivery to tumor vasculature suppresses metastasis. Proc Natl Acad Sci U S A 2008; 105:9343-8; PMID:18607000; http://dx.doi.org/10.1073/pnas.0803728105
10. Manzoor AA, Lindner LH, Landon CD, Park JY, Simnick AJ, Dreher MR, Das S, Hanna G, Park W, Chilkoti A, et al. Overcoming limitations in nanoparticle drug delivery: triggered, intravascular release to improve drug penetration into tumors. Cancer Res 2012; 72:5566-75; PMID:22952218; http://dx.doi.org/10.1158/0008-5472.CAN-12-1683
11. Williams KJ, Telfer BA, Shannon AM, Babur M, Stratford IJ, Wedge SR. Combining radiotherapy with AZD2171, a potent inhibitor of vascular endothelial growth factor signaling: pathophysiologic effects and therapeutic benefit. Mol Cancer Ther 2007; 6:599-606; PMID:17308057; http://dx.doi.org/10.1158/1535-7163.MCT-06-0508
12. Maeda A, Leung MK, Conroy L, Chen Y, Bu J, Lindsay PE, Mintzberg S, Virtanen C, Tsao J, Winegarden NA, et al. In vivo optical imaging of tumor and microvascular response to ionizing radiation. PLoS One 2012; 7:e42133; PMID:22927920; http://dx.doi.org/10.1371/journal.pone.0042133
13. Reitan NK, Thuen M, Goa PE, de Lange Davies C. Characterization of tumor microvascular structure and permeability: comparison between magnetic resonance imaging and intravital confocal imaging. J Biomed Opt 2010; 15:036004; PMID:20615006; http://dx.doi.org/10.1117/1.3431095
14. Palmer GM, Fontanella AN, Shan S, Hanna G, Zhang G, Fraser CL, Dewhirst MW. In vivo optical molecular imaging and analysis in mice using dorsal window chamber models applied to hypoxia, vasculature and fluorescent reporters. Nat Protoc 2011; 6:1355-66; PMID:21886101; http://dx.doi.org/10.1038/nprot.2011.349
15. Baron VT, Welsh J, Abedinpour P, Borgström P. Intravital microscopy in the mouse dorsal chamber model for the study of solid tumors. Am J Cancer Res 2011; 1:674-86; PMID:21994905
16. Speakman JR, Keijer J. Not so hot: Optimal housing temperatures for mice to mimic the thermal environment of humans. Mol Metab 2012; 2:5-9; PMID:24024125; http://dx.doi.org/10.1016/j.molmet.2012.10.002
17. Deer EL, González-Hernández J, Coursen JD, Shea JE, Ngatia J, Scaife CL, Firpo MA, Mulvihill SJ. Phenotype and genotype of pancreatic cancer cell lines. Pancreas 2010; 39:425-35; PMID:20418756; http://dx.doi.org/10.1097/MPA.0b013e3181c15963
18. Otsu N. A Threshold Selection Method from Gray-Level Histograms. IEEE Transactions on Systems, Man and Cybernetics 1979; 9:62-6; http://dx.doi.org/10.1109/TSMC.1979.4310076
19. Arganda-Carreras I, Fernández-González R, Muñoz-Barrutia A, Ortiz-De-Solorzano C. 3D reconstruction of histological sections: Application to mammary gland tissue. Microsc Res Tech 2010; 73:1019-29; PMID:20232465; http://dx.doi.org/10.1002/jemt.20829
20. Potente M, Gerhardt H, Carmeliet P. Basic and therapeutic aspects of angiogenesis. Cell 2011; 146:873-87; PMID:21925313; http://dx.doi.org/10.1016/j.cell.2011.08.039
21. Chang YC, Huang YH, Huang CS, Chang RF. Vascular morphology and tortuosity analysis of breast tumor inside and outside contour by 3-D power Doppler ultrasound. Ultrasound Med Biol 2012; 38:1859-69; PMID:22975041; http://dx.doi.org/10.1016/j.ultrasmedbio.2012.06.010
22. Bullitt E, Zeng D, Gerig G, Aylward S, Joshi S, Smith JK, Lin W, Ewend MG. Vessel tortuosity and brain tumor malignancy: a blinded study. Acad Radiol 2005; 12:1232-40; PMID:16179200; http://dx.doi.org/10.1016/j.acra.2005.05.027
23. Goel S, Duda DG, Xu L, Munn LL, Boucher Y, Fukumura D, Jain RK. Normalization of the vasculature for treatment of cancer and other diseases. Physiol Rev 2011; 91:1071-121; PMID:21742796; http://dx.doi.org/10.1152/physrev.00038.2010
24. Moy AJ, White SM, Indrawan ES, Lotfi J, Nudelman MJ, Costantini SJ, Agarwal N, Jia W, Kelly KM, Sorg BS, et al. Wide-field functional imaging of blood flow and hemoglobin oxygen saturation in the rodent dorsal window chamber. Microvasc Res 2011; 82:199-209; PMID:21787792; http://dx.doi.org/10.1016/j.mvr.2011.07.004
25. Palmer GM, Fontanella AN, Shan S, Dewhirst MW. High-resolution in vivo imaging of fluorescent proteins using window chamber models. Methods Mol Biol 2012; 872:31-50; PMID:22700402; http://dx.doi.org/10.1007/978-1-61779-797-2_3
26. Manning CS, Jenkins R, Hooper S, Gerhardt H, Marais R, Adams S, Adams RH, Van Rheenen J, Sahai E. Intravital imaging reveals conversion between distinct tumor vascular morphologies and localized vascular response to Sunitinib. IntraVital 2013; 2:e24790; http://dx.doi.org/10.4161/intv.24790
27. Barber PR, Vojnovic B, Ameer-Beg SM, Hodgkiss RJ, Tozer GM, Wilson J. Semi-automated software for the three-dimensional delineation of complex vascular networks. J Microsc 2003; 211:54-62; PMID:12839551; http://dx.doi.org/10.1046/j.1365-2818.2003.01205.x
28. Ritsma L, Steller EJA, Ellenbroek SIJ, Kranenburg O, Borel Rinkes IH, van Rheenen J. Surgical implantation of an abdominal imaging window for intravital microscopy. Nat Protoc 2013; 8:583-94; PMID:23429719; http://dx.doi.org/10.1038/nprot.2013.026